Switching between MPPT and VSG Controls for Utility-Scale Photovoltaic Plants to Mitigate Power System Oscillations

Rajan Ratnakumar, IEEE Graduate Student member
Real-Time Power and Intelligent Systems Laboratory
Holcombe Department of Electrical and
Computer Engineering
Clemson University, Clemson, USA.
rajan94@ieee.org

Abstract—The decline of conventional synchronous generators in the modern power system is driven by the increasing demand for low-inertia/inertia-less renewable energy sources (RES), consequently leading to the growing integration of inverter-based resources (IBRs) into the power system. The incorporation of low-inertia/inertia-less IBRs makes the monitoring and damping of low-frequency electromechanical oscillations (EMOs) crucial. While Virtual Synchronous Generator (VSG) control introduces virtual inertia into the power system, it does not maximize energy capture from RES as effectively as maximum power point tracking (MPPT) does, as it should maintain a power reserve to provide the inertial support and damping. In this study, switching IBRs between MPPT and VSG controls based on an EMO index (EMOI) threshold is proposed to mitigate the emergence of EMO. The impact of the switching control of IBRs is illustrated for a modified two-area, four-machine power system with two large solar photovoltaic plants. Typical results are presented from a simulation on real-time digital simulator (RTDS) to show improved EMOI.

Keywords— Electromechanical oscillations, inverter-based resources, stability, switching control, virtual inertia.

I. INTRODUCTION

The modern power system, incorporating diverse nonlinear components and an increasing number of renewable energy sources (RES), faces significant challenges. The decline in shares of synchronous generators is primarily driven by the escalating demand for renewable energy sources, resulting in a notable surge of inverter-based resources (IBRs) in the power system [1]-[3]. The power system's stability is decreasing with the growing integration of conventional IBRs due to their lack of inherent rotational inertia. This becomes more critical as IBRs, commonly found in renewables like solar and wind, become a larger part of the energy mix, necessitating additional security measures for grid stability.

Recently, various studies have proposed virtual inertia as a solution. The Australian power system has been investigated, with a specific focus on addressing low inertia challenges in [4]. This study reviewed the measures implemented by regulatory authorities and investigates the potential of variable-speed wind generators and energy storage systems in frequency regulation. An important aspect emphasized is the concept of virtual inertia, where IBRs mimic the stabilizing effect of traditional rotating mass. This is critical in modern power systems with increased RES and reduced system inertia. While these technologies have proven effective, further research is needed to fine-tune

This research was funded by US NSF grants (CNS 2131070, ECCS 2234032, and CNS 2318612) and the Duke Energy Distinguished Professor Endowment Fund.

Ganesh K. Venayagamoorthy, IEEE Fellow
Real-Time Power and Intelligent Systems Laboratory
Holcombe Department of Electrical and Computer
Engineering, Clemson University, Clemson, USA.
Department of Electrical, Electronic and Computer
Engineering, University of Pretoria, South Africa.
gkumar@ieee.org

control parameters, provide detailed algorithms, and develop accurate methods for quantifying system inertia, especially in the context of IBR-based power plants. A virtual synchronous generator (VSG) control scheme was introduced in [5] to enhance power system stability by emulating synchronous machine behavior. The VSG design incorporates the swing equation, allowing real-time control of parameters to improve rapid frequency response. An alternating moment of inertia approach was presented with transient energy analysis.

As noted, the incorporation of low-inertia IBRs necessitates the monitoring and damping of low-frequency electromechanical oscillations (EMOs) in power systems. Undamped oscillations can make the power system vulnerable to instability and hamper its secure operation. The EMOs can intensify following one or more severe disturbances. Hence, it is important to consistently monitor and integrate new damping measures to ensure secure power system operations [6]. The study in [7] explored the impact of substituting traditional synchronous generators (SGs) with VSGs on EMOs. It compares their modeling and establishes a general small-signal model representing both SGs and VSGs, incorporating frequency and voltage regulation. Through comprehensive small-signal analysis, the influence of VSG states on EMOs is presented.

The disadvantage of using VSG control instead of maximum power point tracking (MPPT) control in solar PV plants without energy storage is that VSG does not maximize energy capture from RES as effectively as MPPT. The study in [8] proposed a novel VSG control for photovoltaic (PV) systems, providing frequency support without energy storage. This approach reserves PV power based on a predefined curve and operates away from the MPPT to enhance stability. So, a VSG control without energy storage prioritizes power system stability, potentially sacrificing some energy harvest by keeping power reserve in comparison to dedicated MPPT algorithms.

An online hierarchical EMO index (EMOI), ranging between 0 and 1, that combines time response analysis (TRA) and frequency response analysis (FRA) was introduced in [9] and used in [10] to create operational situational awareness (OpSA) in energy control centers. This index provides an indication and can be used to flag the level of security of a power system due to EMOs, especially from severe disturbances. A new method for defining an EMOI-based stability threshold (*EMOI_{th}*) and utilizing it in performing stability-constrained contingency analysis (SCCA) was presented in [11].

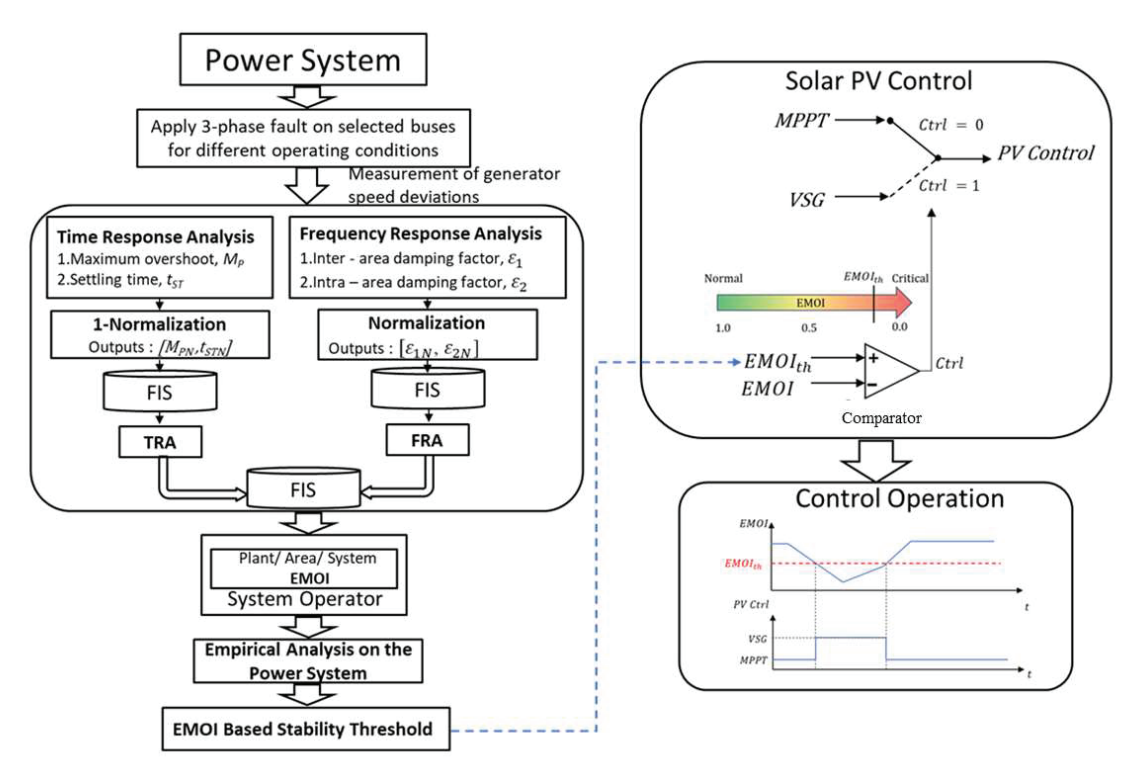


Fig. 1. MPPT - VSG switching control and definition of the EMOI based stability threshold.

In this paper, IBR switching control between MPPT and VSG is investigated in order to mitigate the effects of EMOs when the power system is operating in vulnerable conditions and maximize the energy capture for the PV plant during normal and abnormal conditions. The EMOI and $EMOI_{th}$ is used as a measure to monitor this vulnerability and keep the "duty cycle" of the VSG switching control mode to a minimum, thus not curtailing/wasting the PV plant power output.

The primary contributions of this paper are as follows:

- Development and implementation of a switching control strategy between maximum power point tracking and virtual synchronous generator control to damp electromechanical oscillations while maximizing the energy capture from RESs in modern power systems.
- Implementation and performance evaluation of the MPPT-VSG switching control strategy on a modified two-area, four-machine power system with two large solar photovoltaic plants simulated on a real-time digital simulator (RTDS).

II. DEVELOPMENT OF THE MPPT-VSG SWITCHING CONTROL

The development of the MPPT-VSG Switching Control and the test system is discussed in the subsections. The comprehensive switching operation is shown in Fig.1.

A. VSG Control

The inverter controls consist of a real power control loop and a reactive power control loop, and it will produce the phase angle, θ , and voltage magnitude needed for the PWM. The primary distinction between MPPT control and VSG control lies in the management of real power, which ultimately determines the phase angle. Virtual inertia control is used to emulate the behavior of synchronous generators, which provide inherent inertia to the grid. By incorporating virtual inertia control, grid-forming inverters can respond to sudden changes in power demand and maintain grid stability. The real power control mechanism for VSG is illustrated in Fig. 2.

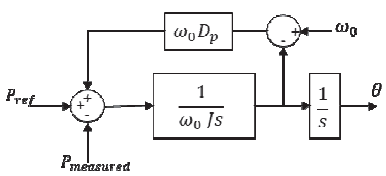


Fig. 2. VSG Control of the Solar PV System.

Like real synchronous generators, the frequency response output in a VSG is influenced by the phase angle of the voltage output. This phase angle is determined by the reference real power, rated frequency, damping coefficient, and virtual inertia settings, as described by the swing equation below:

$$J\frac{d\omega}{dt} = T_m - T_e - D_p \left(\omega - \omega_0\right) \approx \frac{P_m - P_e}{\omega_0} - D_p \left(\omega - \omega_0\right) \tag{1}$$

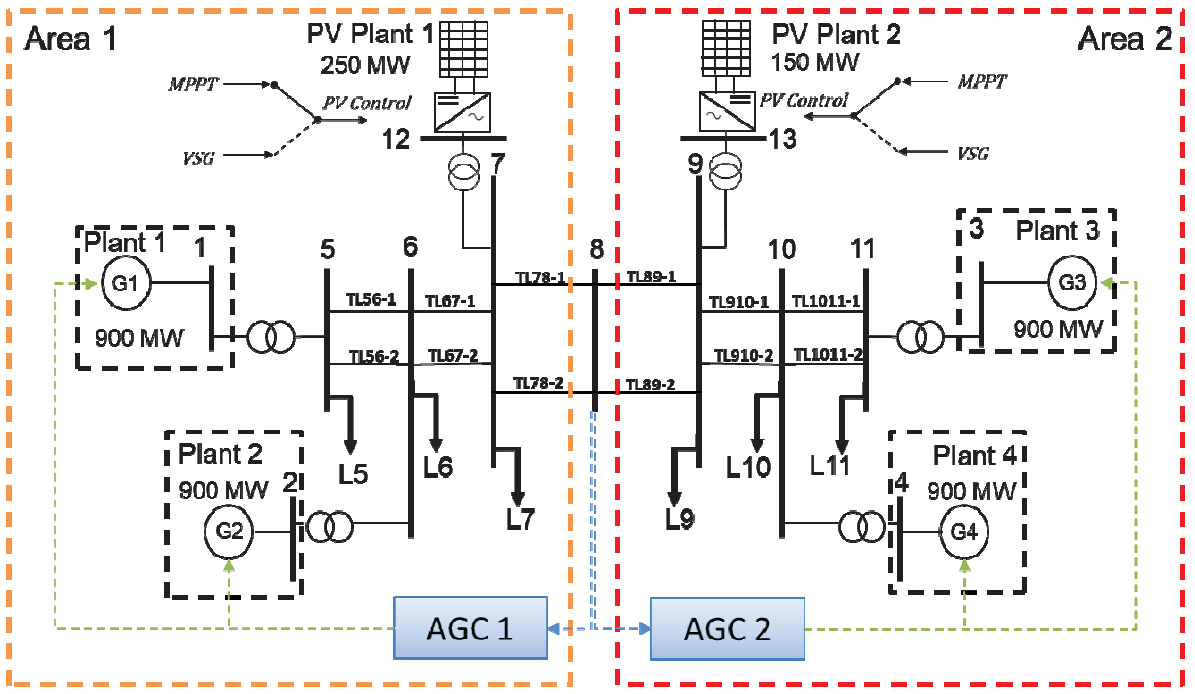


Fig. 3. Modified two-area four- machine power system with two large solar photovoltaic plants and automatic generation controls (AGCs).

Where J is the virtual moment of inertia, T_m and T_e are the virtual mechanical torque and electrical torque, respectively, D_n is the damping factor.

B. MPPT-VSG Switching Control

Authors in [11] has proposed a stability-constrained contingency analysis (SCCA) method that integrates an EMOI based stability threshold (EMOIth) to enhance grid security in modern power systems. Here in MPPT-VSG switching control, the EMOIth is used as a threshold to switch between MPPT and VSG control modes.

The TRA is obtained using Takagi-Sugeno (TS) fuzzy logic, with two inputs: normalized maximum overshoot (M_{PN}) and normalized settling time (t_{STN}) . M_{PN} and t_{STN} denote the normalized maximum overshoot and settling time, respectively, while M_P and t_{ST} represent their maximum actual values. NF_{MP} and NF_{tST} are the associated normalization factors. Normalization is carried out because larger values of maximum overshoot and settling time indicate worse conditions.

Similarly, inter-area and intra-area damping factors of the signal are normalized, and the FRA is obtained using TS fuzzy logic, with two inputs: normalized inter-area damping factor (ε_{IN}) and normalized intra-area damping factor (ε_{2N}), along with nine simplified rules. ε_{IN} and ε_{2N} denote the normalized inter-area and intra-area damping factors, respectively, while ε_1 and ε_2 represent their actual values. $NF_{\varepsilon 1}$ and $NF_{\varepsilon 2}$ stand for the associated normalization factors. The EMOI is obtained by integrating the estimated TRA and FRA components using TS fuzzy logic.

The power system operator will monitor the EMOIs, determining when to switch control of the Solar PV plants between MPPT and VSG based on the EMOI threshold, indicating the stability for EMOs in the power system as shown in Fig. 1.

C. Modified Two-Area Four-Machine Power System

The modified two-area, four-machine power system [12] shown in Fig. 3 is used as the test power system to demonstrate the VSG control model and is simulated in realtime on the real-time digital simulator (RTDS) [13]. The power system has four power plants including ten generators and two solar photovoltaic power plants in two areas. The solar PV plants in Area 1 and Area 2 are rated 250 MWp and 150 MWp, respectively and can be switched between MPPT and VSG control. The generation of Area 1 and Area 2 is regulated by two automatic generation controllers (AGCs).

III. RESULTS AND DISCUSSION

The performance of MPPT and VSG control switching are evaluated on the modified two-area four-machine power system for different cases. Case 1 represents switching at a normal condition and Case 2 represents switching at a critical stage. The stability is evaluated by applying a three - phase 10 cycles faults at selected buses. Here, the EMOI threshold value is selected as 0.5.

The transient energies of generators are calculated, and normalized values of transient energies are computed to compare different scenarios (t_f - t_s = 10 s, given in (2a)). The normalized transient energy of a generator for a specific fault is determined by dividing the generator's transient energy by the maximum transient energy observed among all generators for that fault in the given case, as described in (2b).

$$T.E_{G_{i}} = \sum_{t_{s}}^{t_{f}} 0.5 * H_{G_{i}} \Delta \omega_{G_{i}}^{2}$$

$$Normalized T.E_{G_{i}} = \frac{T.E_{G_{i}}}{\max(T.E_{G_{1}}, T.E_{G_{2}}, \dots T.E_{G_{n}})}$$
(2a)

Normalized
$$T.E_{G_i} = \frac{T.E_{G_i}}{\max(T.E_{G_1}, T.E_{G_2}, \dots T.E_{G_n})}$$
 (2b)

A. Case 1: MPPT-VSG Switching in Normal Scenario

The performance of the MPPT control and VSG control during normal operation is analyzed in this case. Here, the EMOI is above the *EMOI*_{th} value, and is investigated to evaluate the impact of VSG control on the EMO. A three-phase, 10-cycle fault is applied at selected buses while the Solar PV Plant is operated with MPPT or VSG control. The EMOI is then assessed to evaluate the performance of VSG on EMO damping. Herein, the solar PV Plant 1 is operating 50 % of its maximum power.

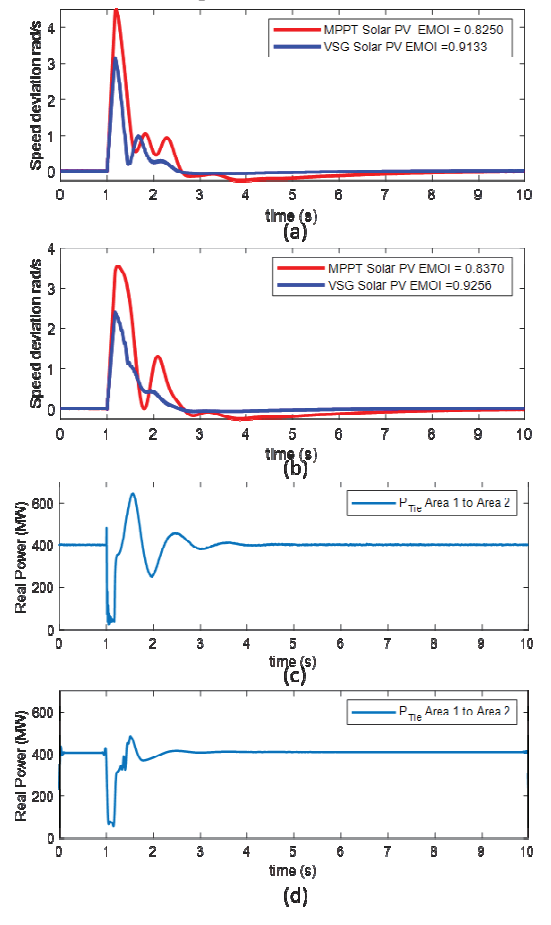


Fig. 4. Speed deviation of (a) Plant 1 (b) Plant 2 with 10 cycles fault at Bus 8 with MPPT and VSG controls. (c) Tie-line power flow with MPPT control (d) Tie-line power flow with VSG control.

Figs. 4 (a) and (b) present the speed variations of Plant 1 and Plant 2 during a 10-cycle fault at Bus 8, with Solar PV Plant 1 controlled with MPPT and VSG modes. Figs. 4 (c) and (d) show the tie-line power flow with MPPT and VSG for the fault. Similarly, Figs. 5 (a) and (b) illustrate the speed variations of Plant 1 and Plant 2 during a 10-cycle fault at Plant 3, Bus 3. The results highlight a notable improvement in damping and Plant EMOIs with the application of the VSG control despite the PV plant operating at 50% of its maximum power.

The enhancement in damping and Plant EMOIs is significant. VSG control, by emulating synchronous generator characteristics, provides better inertia and damping, essential for mitigating oscillations. The results clearly show that VSG control, even at 50% PV plant

capacity, significantly contributes to stability. The comparison of the Plant EMOI is given in Table I.

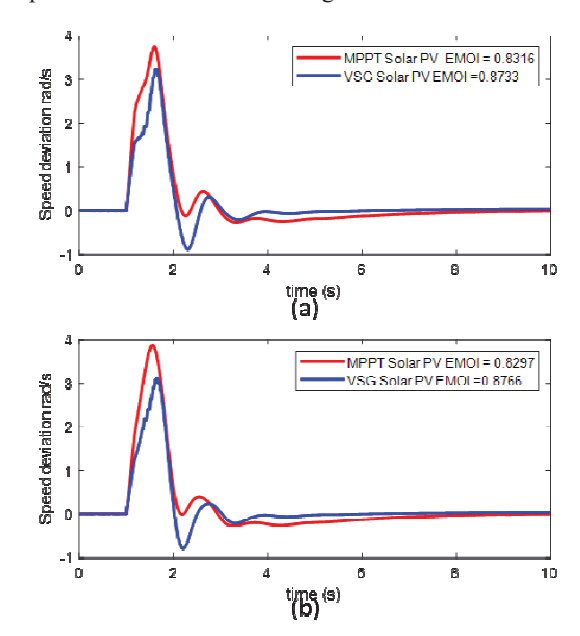


Fig. 5. Speed deviation of (a) Plant 1 (b) Plant 2 with 10 cycles fault at Plant 3 Bus with MPPT and VSG controls.

B. Case 2: MPPT-VSG Switching in Critical Scenario

Case 2 evaluates the performance of the MPPT- VSG switching control in a critical scenario where the loss of TL89-1 pushes the EMOI below the threshold. A three-phase, 10-cycle fault is applied at selected buses while the Solar PV Plant is operated with MPPT and VSG control modes. The EMOI is then assessed to evaluate the performance of VSG on EMO damping. Herein, the solar PV Plant 1 was operating at 40 % of its maximum power to enhance the EMOI.

Figs. 6 (a) and (b) present the speed variations of Plant 1 and Plant 2 during a 10-cycle fault at Bus 8 when Solar PV Plant 1 is controlled with MPPT and VSG modes when the transmission line TL89-1 is disconnected, a line contingency. Figs. 6 (c) and (d) show the tie-line power flow with MPPT and VSG control models for the fault. Similarly, Figs. 7 (a) and (b) illustrate the speed variations of Plant 1 and Plant 2 during a 10-cycle fault at Plant 3, Bus 3, when the transmission line TL89-1 is disconnected.

After the loss of line TL89-1, the EMOI is in its threshold limit for the fault at Plant 3, Bus 3, whereas it drops below the threshold (*EMOIth*) for the fault at Bus 8. In this situation, the switching control transitions from the MPPT operation mode to the VSG operation mode. This transition improves the EMOI, thereby restoring the system from critical mode to normal mode concerning electromechanical oscillation damping stability.

However, the Solar PV Plant 1 can only operate at 40% of its rated capacity to support the EMO damping. Once the situation is restored to normal, the system can switch back to MPPT mode, ensuring that the PV plant power output is not curtailed or wasted.

The comparison of the Plant EMOI and T.Es is given in Table I.

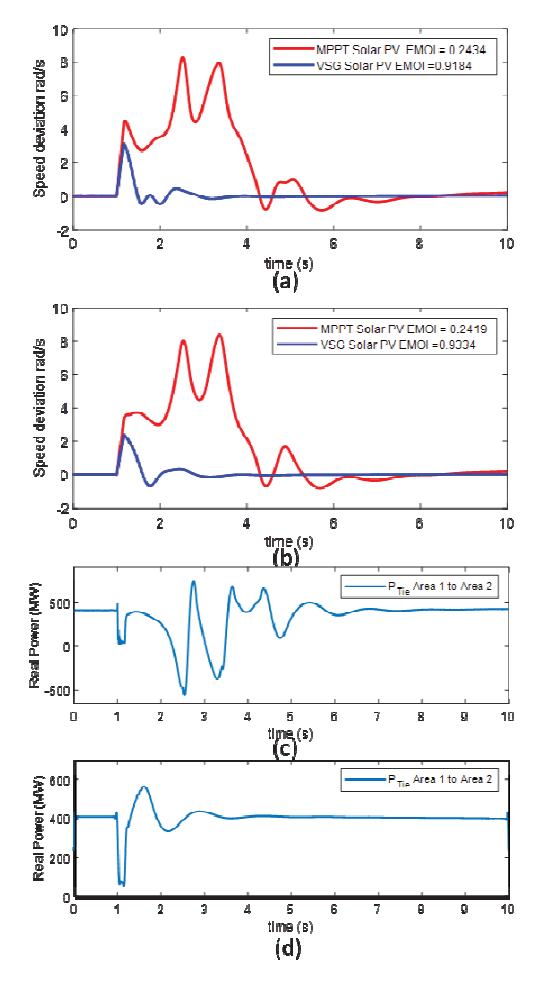


Fig. 6. Speed deviation of (a) Plant 1 (b) Plant 2 with 10 cycles fault at Plant 3 Bus with MPPT and VSG controls while line loss between Bus 8 and 9 (c) Tie-line power flow with MPPT control (d) Tie-line power flow with VSG control

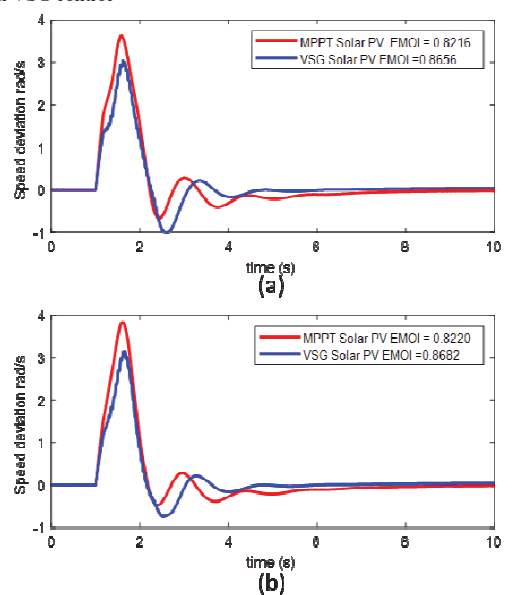


Fig. 7. Speed deviation of (a) Plant 1 (b) Plant 2 with 10 cycles fault at Plant 3 Bus with MPPT and VSG controls

TABLE I. COMPARISON OF MPPT AND VSG APPROACHES

Case	Plant	Control Approach		for a Fault at	Plant EMOI for a Fault at Bus 3		
			Plant EMOI	Normalized T.E	Plant EMOI	Normalized T.E	
	Plant 1	MPPT	0.8250	0.679	0.8316	0.574	
Case 1	Plant I	VSG	0.9133	0.190	0.8733	0.361	
	Plant 2	MPPT	0.8370	1.000	0.8297	0.899	
		VSG	0.9256	0.244	0.8766	0.534	
	Plant 3	MPPT	0.7585	0.705	0.6756	0.872	
		VSG	0.8637	0.192	0.6900	0.835	
	Plant 4	MPPT	0.7336	0.811	0.6636	1.000	
		VSG	0.8389	0.236	0.6978	0.867	
Case 2	Plant 1	MPPT	0.2434	0.669	0.8216	0.558	
		VSG	0.9184	0.017	0.8659	0.359	
	Plant 2	MPPT	0.2419	1.000	0.8220	0.865	
		VSG	0.9324	0.020	0.8682	0.526	
	Plant 3	MPPT	0.1582	0.285	0.6601	0.867	
		VSG	0.9334	0.008	0.6789	0.828	
	Plant 4	MPPT	0.2456	0.248	0.8029	1.000	
		VSG	0.9201	0.009	0.8556	0.923	

IV. CONCLUSION

The modern power system, evolving with many low inertia inverter-based renewable energy sources, necessitates advanced control methods like VSG to introduce virtual inertia. However, VSG control will not optimize energy capture from renewables as MPPT. A switching control between VSG and MPPT controls based on situational awareness of EMOs has been presented to mitigate the emergence of EMOs while maximizing energy capture. The switching of control modes can be further optimized by using an artificial intelligence-based technique that learns the system and provides optimal reconfiguration of the control mode to maximize stability while maximizing clean energy capture.

ACKNOWLEDGEMENT

This research was funded by US NSF grants (CNS 2131070, ECCS 2234032, and CNS 2318612) and the Duke Energy Distinguished Professor Endowment Fund.

REFERENCES

- H. Liu, L. Jin, D. Le and A.Chowdhury, "Impact of highpenetration of solar photovoltaic generation on power systemsmall signal stability", in Proc. 2010 POWERCON, pp. 1-7 2010.
- [2] D. S. Kumar, A. Sharma, D. Srinivasan and T. Reindl, "Stability implications of bulk power networks with large scale pvs", Energy, vol. 187, pp. 1-15, Nov. 2019.
- [3] J.Song, X. Zhou, Z. Zhou, Y. Wang and X.Wang, "Review of Low Inertia in Power Systems Caused by High Proportion of Renewable Energy Grid Integration," Energies, 2023,16(16), p.6042.
- [4] T. T. To and M. H. Haque, "Inertia Shortfall and the Capability of Inverter-based Generation to provide Inertial Response: A Review for Australian Power System," 2021 31st Australasian Universities Power Engineering Conference (AUPEC), Perth, Australia, 2021.
- [5] J. Alipoor, Y. Miura and T. Ise, "Power System Stabilization Using Virtual Synchronous Generator With Alternating Moment of Inertia," in IEEE Journal of Emerging and Selected Topics in Power Electronics, vol. 3, no. 2, pp. 451-458, June 2015.
- [6] F. Hauer, D. J. Trudnowski, and J. G. DeSteese, "A perspective on WAMS analysis tools for tracking of oscillatory dynamics," in Proc.2007 IEEE Power Eng. Soc. General Meeting, Tampa, FL, Jun. 2007.
- [7] M. Chen, D.Zhou. and F. Blaabjerg, "High penetration of inverter-based power sources with VSG control impact on electromechanical oscillation of power system." *International Journal of Electrical Power & Energy Systems*, 2022.
- [8] C. Zhong, H. Li, Y. Zhou, Y. Lv, J. Chen and Y. Li, "Virtual synchronous generator of PV generation without energy storage for

- frequency support in autonomous microgrid," *International Journal of Electrical Power & Energy Systems*, vol. 134, pp. 107343 2022.
- [9] J. Richards, R.Ratnakumar G. K. Venayagamoorthy, "An Online Electromechanical Oscillation Index for a Modern Bulk Power System," CIGRE US National Committee, Grid of the Future Symposium, 2022.
- [10] R.Ratnakumar, J. Richards, G. K. Venayagamoorthy, "Modern control center operational situational awareness considering electromechanical oscillations," 2023 IEEE AFRICON, Nairobi, Kenya, 2023.
- [11] R. Ratnakumar and G. K. Venayagamoorthy, "Stability-Constrained Contingency Analysis for Modern Power Systems," 3rd Control Conference Africa (CCA), IFAC, 2024.
- [12] P. Kundur, *Power System Stability and Control.* New York, NY, USA: McGraw-Hill, 1994.

Appendix A

TABLE A.1. GENERATION DATA

Generation Data (MW)								
DI (D)	Area 1			Area 2			Tie line flow from	
Plant Parameters	P1	P2	PV1	Р3	P4	PV2	Area 1 to Area 2 (MW)	
Inertia (s)	3	4.5	-	3.45	2.65	-		
Rating (MVA)	900	900	250	900	900	150	406	
Participation factor	0.5	0.5	-	0.5	0.5	-		
	620	620	250	615	615	150		
Generation (MW)	1490		1380					
			28	370				

TABLE A.2. LOAD DATA

Load Data (MW)							
	Area 1		Area 2				
Bus 5	Bus 6	Bus 7	Bus 9	Bus 10	Bus 11		
557	353	170	552	710	505		
	1080		1767				
2847							